AIP Journal of Applied Physics

Upconversion luminescence in Er3+ doped Ga10Ge25S65 glass and glass-ceramic excited in the near-infrared

Whualkuer Lozano B., Cid B. de Araújo, Yannick Ledemi, and Younes Messaddeq

Citation: Journal of Applied Physics **113**, 083520 (2013); doi: 10.1063/1.4793638
View online: http://dx.doi.org/10.1063/1.4793638
View Table of Contents: http://scitation.aip.org/content/aip/journal/jap/113/8?ver=pdfcov
Published by the AIP Publishing

Upconversion luminescence in Er^{3+} doped $Ga_{10}Ge_{25}S_{65}$ glass and glass-ceramic excited in the near-infrared

Whualkuer Lozano B.,[1,a)] Cid B. de Araújo,[1,b)] Yannick Ledemi,[2,3] and Younes Messaddeq[2,3]
[1]*Departamento de Física, Universidade Federal de Pernambuco, Recife-PE 50670-901, Brazil*
[2]*Centre d'Optique, Photonique et Laser, Université Laval, Québec (Qc) G1V 0A6, Canada*
[3]*Instituto de Química, Universidade Estadual Paulista-UNESP, 14801-970 Araraquara, São Paulo, Brazil*

(Received 21 November 2012; accepted 13 February 2013; published online 27 February 2013)

The infrared-to-visible frequency upconversion was investigated in Er^{3+}-doped $Ga_{10}Ge_{25}S_{65}$ glass and in the transparent glass-ceramic obtained by heat-treatment of the glass above its glass-transition temperature. Continuous-wave and pulsed lasers operating at 980 nm and 1480 nm were used as excitation sources. The green ($^2H_{11/2} \rightarrow {}^4I_{15/2}$; $^4S_{3/2} \rightarrow {}^4I_{15/2}$) and red ($^4F_{9/2} \rightarrow {}^4I_{15/2}$) photoluminescence (PL) signals due to the Er^{3+} ions were characterized. The PL decay times were influenced by energy transfer among Er^{3+} ions, by cross-relaxation processes and by energy transfer from the Er^{3+} ions to the host material. The PL from the Er^{3+} ions hosted in the crystalline phase was distinguished only when the glass-ceramic was excited by the 1480 nm pulsed laser. The excitation pathways responsible for the green and red PL bands are discussed to explain the differences between the spectra observed under continuous-wave and pulsed excitation. © *2013 American Institute of Physics*. [http://dx.doi.org/10.1063/1.4793638]

I. INTRODUCTION

The search of transparent materials that can be doped with rare earth (RE) ions has been very intense in the past years motivated by applications in displays, biomedical lasers, optical sensors, optical amplifiers, among other uses.[1–6] In particular, special glasses and glass-ceramics are being increasingly studied because they have unique features such as large acceptance for high RE ions doping concentration, large optical homogeneity, wide transparency from the visible to the infrared region, high mechanical strengths and simple manufacture procedures for obtaining good optical quality samples. Among the materials that exhibit such appropriate characteristics for photonics are the chalcogenide glasses and chalcogenide glass-ceramics that exhibit high refractive index (≈2.2), low cutoff phonon energy (≈400 cm^{-1}), and high stability against moisture and devitrification.[2–6]

In previous papers, we reported on the photoluminescence (PL) properties of the chalcogenide glass $Ga_{10}Ge_{25}S_{65}$ (GGS) doped with Nd^{3+}, Pr^{3+}, and Er^{3+} ions. For the Nd^{3+}-doped GGS glass (GGS-GLASS), we determined transition probabilities, radiative lifetimes, and branching ratios related to the Nd^{3+} ions. Green and red emissions were observed for excitation at 1064 nm due to two-photon absorption by isolated ions and energy transfer among Nd^{3+} pairs.[7] In Pr^{3+}-doped GGS glasses, we observed orange-to-blue frequency upconversion (UC) and investigated the influence of silver nanoparticles on the UC efficiency.[8] The UC enhancement observed was attributed to the large local field acting on the Pr^{3+} ions due to their proximity with silver nanoparticles. Er^{3+}-doped GGS glass was studied under laser excitation at 532 nm, 800 nm, and 980 nm.[9] Er^{3+} parameters such as transition probabilities, radiative lifetimes, and branching ratios were determined. Also, the mechanisms leading to Stokes and anti-Stokes PL were discussed. Other authors investigated the UC luminescence in Er^{3+}-doped GGS-CsCl glass-ceramic excited at 800 nm.[10] Enhancements of the green and red PL were observed in comparison with the base-glass.

In the present article, we report on the infrared-to-visible UC luminescence of Er^{3+}-doped GGS glass and Er^{3+}-doped GGS glass-ceramics (GGS-GC) excited at 980 nm and 1480 nm. The experiments were performed with continuous-wave (CW) and pulsed lasers. The intensity and the time behavior of the visible PL due to the Er^{3+} ions were studied. The excitation mechanisms contributing for the UC process and for the relaxation rates of the electronic states involved in the PL process are discussed.

II. EXPERIMENTAL DETAILS

The base-glass (GGS-GLASS) with composition $Ga_{10}Ge_{25}S_{65}$:$(Er_2S_3)_{0.25}$ (mol. %) was prepared by the melt-quenching method using a mixture of highly pure raw materials (Ga_2S_3, Ge, S: 99.99% and Er_2S_3: 99%) in a silica ampoule sealed under vacuum (10^{-4} mbar). The ampoule of 9 mm inner diameter was placed in a rocking furnace, slowly heated up to 900 °C and maintained at this temperature for 12 h. The silica tube was quenched in water at room temperature, annealed near the glass transition temperature, T_g, for 3 h to minimize inner constraints, and finally slowly cooled down to room temperature. The glass rods of 8 g weight were cut into slices of 2 mm thickness and polished to obtain perpendicular polished faces for the optical measurements. The value of $T_g = 430$ °C, and the onset crystallization

[a)]Permanent address: Facultad de Ciencias Físicas, Universidad Nacional Mayor de San Marcos-UNMSM, Lima, Peru.
[b)]Author to whom correspondence should be addressed. Electronic mail: cid@df.ufpe.br.

temperature, $T_x = 540\,^{\circ}C$ were determined by differential scanning calorimetry, with a heating rate of 10 °C/min. A description of the fabrication procedure is presented in Refs. 11 and 12.

The glass-ceramics (GGS-GC) were prepared by heat-treatment of polished slices of the base-glass at 450 °C for 15 h. The volume crystallization was checked by X ray diffraction and transmission electron microscopy that demonstrate the presence of Ga_2S_3 nanocrystals as reported in Refs. 10–12. The samples were optically homogeneous to the naked eye.

The linear optical absorption spectra were recorded using a commercial spectrophotometer.

For the PL experiments with excitation at 980 nm (10 204 cm^{-1}) and 1480 nm (6757 cm^{-1}), CW diode lasers (chopped at 8 Hz) with maximum output power of 300 mW and one optical parametric oscillator (5 ns, 5 Hz) pumped by a Nd: YAG laser were used. In all cases, the beams were focused onto the samples using a lens with focal length of 10 cm. The PL signals collected along a direction perpendicular to the laser beam were dispersed by a 0.25 m grating spectrometer attached to a photomultiplier tube. The signals were recorded using a digital oscilloscope connected to a personal computer. All measurements were made at room temperature.

III. RESULTS AND DISCUSSION

A. Linear absorption spectra and CW laser excitation

Figure 1 shows the absorbance spectra of the GGS-GLASS and the GGS-GC samples. The bands centered at ≈492 nm, ≈526 nm, ≈547 nm, and ≈661 nm are due to transitions from the ground state ($^4I_{15/2}$) to the excited states $^4F_{7/2}$, $^2H_{11/2}$, $^4S_{3/2}$, and $^4F_{9/2}$, respectively. The bands related to the Er^{3+} ion states with higher energies than the $^4F_{7/2}$ state cannot be seen because they lie above the absorption edge of the samples. The bands' positions in Fig. 1 are in agreement with the ones observed in other Er^{3+} doped glasses[1–3,10,13,14] and the spectrum in the infrared region was already presented in Ref. 9. All Er^{3+} transitions are inhomogeneously broadened due to site-to-site variations of the crystalline field. Notice that the GGS-GC absorption edge is red-shifted with respect to the GGS-GLASS; it is an indication that the crystallization of the inner crystalline phase has been completed after 15 h of heat-treatment.[11] The optical gap energy, E_g, for both samples was determined from Fig. 1 by plotting the square of the optical absorption coefficient, α_0^2, versus the photon energy and determining the crossing point between a straight line fitted to the α_0^2 curve and the horizontal axis. The results obtained were $E_g = 2.42$ eV (19 526 cm^{-1}) for the GGS-GLASS and $E_g = 2.40$ eV (19 353 cm^{-1}) for the GGS-GC.

Typical UC spectra under CW laser excitation at 980 nm and at 1480 nm emitted by the GGS-GLASS and GGS-GC are shown in Figs. 2(a) and 2(b), respectively. The PL bands centered at ≈660 nm, ≈549 nm, and ≈530 nm are due to the Er^{3+} transitions $^4F_{9/2} \rightarrow {}^4I_{15/2}$, $^4S_{3/2} \rightarrow {}^4I_{15/2}$, and $^2H_{11/2} \rightarrow {}^4I_{15/2}$, respectively. The amplitude of the green (red) signal is ≈1000% (≈100%) times larger for excitation at 980 nm than at 1480 nm. A very weak emission centered at ≈493 nm [$^4F_{7/2} \rightarrow {}^4I_{15/2}$] was observed only for excitation at 980 nm which is resonant with transitions $^4I_{15/2} \rightarrow {}^4I_{11/2}$ and $^4I_{11/2} \rightarrow {}^4F_{7/2}$. However, the signal-to-noise ratio was poor and cannot be clearly observed in Fig. 2.

The intensity ratio ($R = I_{549\,nm}/I_{530\,nm}$) between the two green PL bands excited at 980 nm was twice higher than the

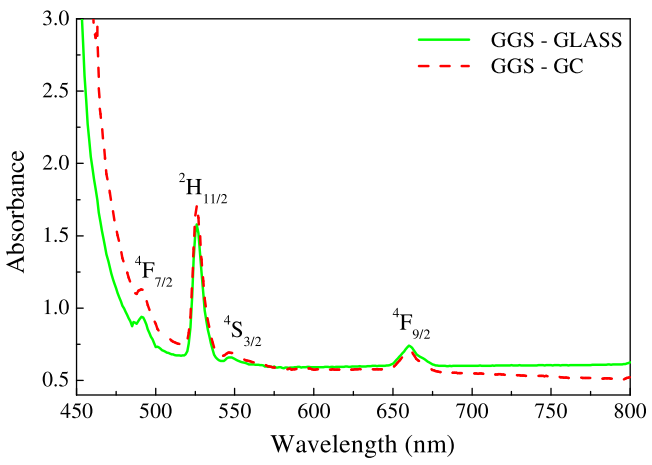

FIG. 1. Absorbance spectra of the GGS-GLASS (green solid line) and GGS-GC (red dashed line). Sample thickness: 2 mm.

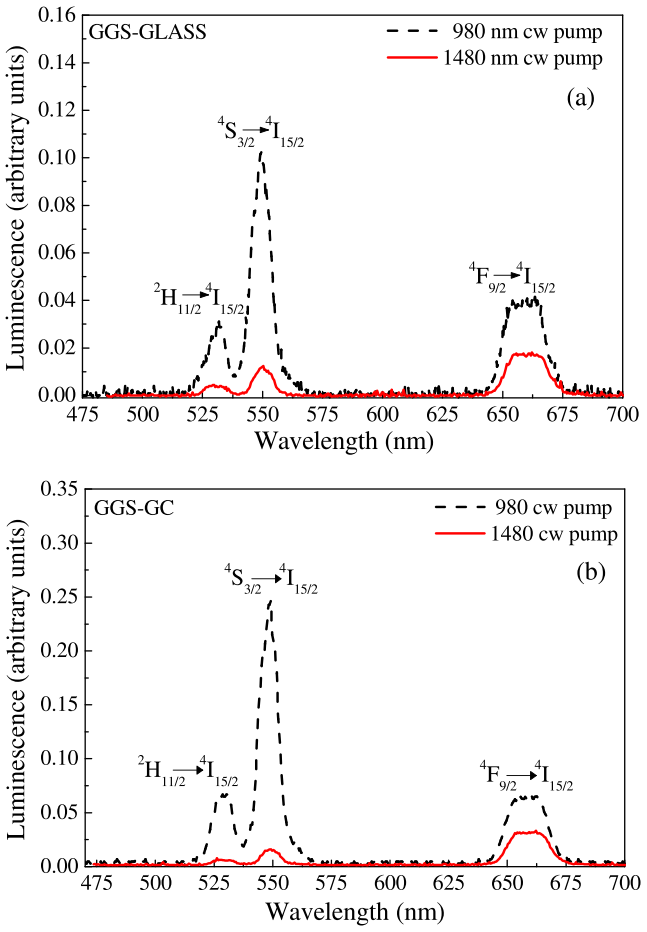

FIG. 2. Room temperature UC emission spectra obtained for excitation at 980 nm and 1480 nm with continuous-wave lasers: (a) GGS-GLASS; (b) GGS-GC.

one obtained with excitation at 1480 nm. The reason for this discrepancy is attributed to the dominant UC mechanism in each case, as discussed below. The green PL is visible to the naked eye for 1480 nm CW laser powers higher than 10 mW; however, it is weaker when the pulsed laser at 1480 nm was used.

The dependence of the UC intensity, I_{UC}, versus the laser intensity, I, in the absence of saturation, is described by $I_{UC} \propto I^N$, where N is the number of photons that participate in the UC process. Hence, the value of N corresponding to each UC transition was obtained from the slope of the straight line representing I_{UC} versus I in the double-logarithmic plot of Fig. 3. It is shown in Figs. 3(a) and 3(b) that the laser intensity dependence of the green and the red PL bands when excited at 1480 nm presents cubic power law corresponding to the absorption of three laser photons. Fig. 3(c), for excitation at 980 nm, shows quadratic dependence of I_{UC} versus I indicating that two laser photons contribute for the UC process in the GGS-GC. The results for the GGS-GLASS sample were reported in Ref. 9 and also present quadratic dependence.

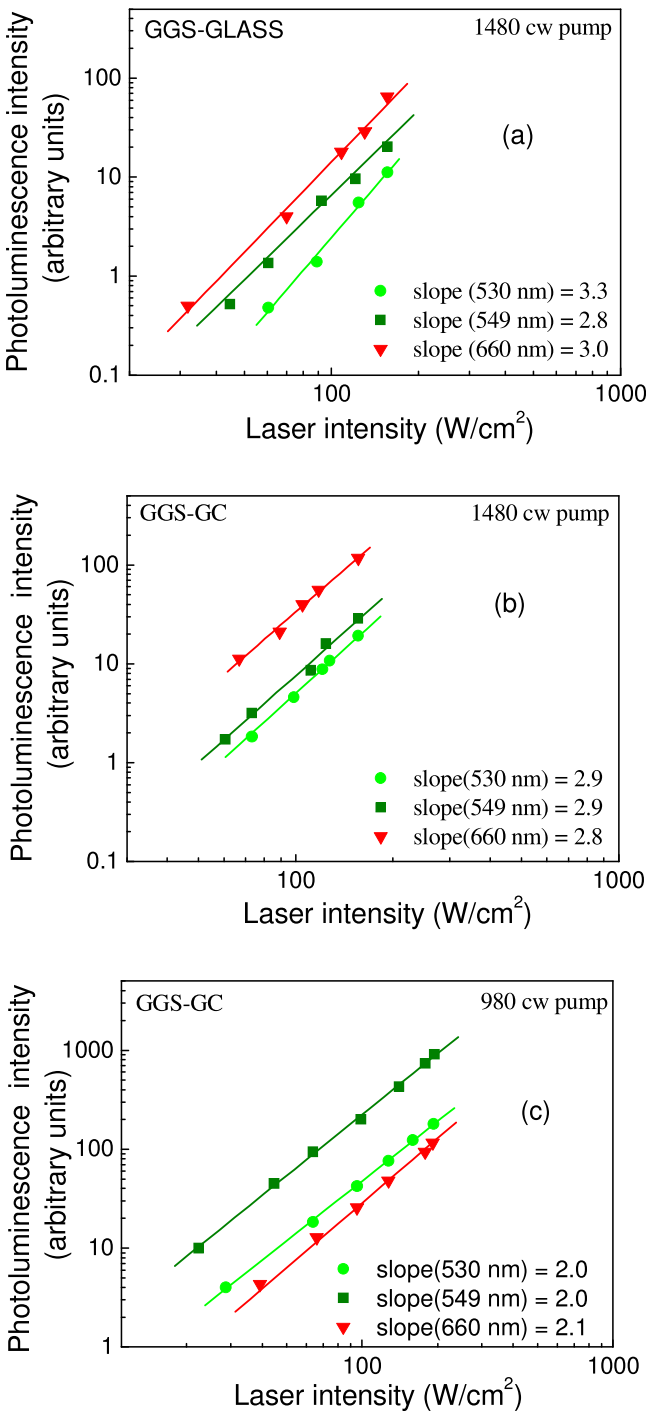

FIG. 3. Photoluminescence intensity versus laser intensity. Excitation wavelength: 1480 nm (a) and (b); 980 nm (c).

Figure 4 shows the relevant Er^{3+} energy levels together with indication of possible UC pathways for both excitation wavelengths and the observed PL lines. A simplified scheme of the conduction and valence bands of the host matrix is also shown in Fig. 4.

The main processes that may lead to transitions involving the excited Er^{3+} ion states in experiments with low-power infrared lasers are excited state absorption, cross-relaxation (CR), and energy transfer (ET) among the ions. Another possibility would be the excitation of the host matrix by multiphoton absorption followed by ET from the matrix to the Er^{3+} ions; however, this process is less probable than the one mentioned above. Nevertheless it is important when high-power lasers are used as shown in Sec. III B.

For excitation at 980 nm, the laser wavelength is in resonance with the transitions $^4I_{15/2} \rightarrow {}^4I_{11/2}$ and $^4I_{11/2} \rightarrow {}^4F_{7/2}$. Then, after promotion of Er^{3+} ions to level $^4F_{7/2}$, nonradiative (NR) decay to levels $^2H_{11/2}$ and $^4S_{3/2}$ takes place followed by the green emissions due to transitions $^4S_{3/2} \rightarrow {}^4I_{15/2}$ and $^2H_{11/2} \rightarrow {}^4I_{15/2}$. The red emission (transition $^4F_{9/2} \rightarrow {}^4I_{15/2}$) is due to the population that reached level $^4F_{9/2}$ by phonon relaxation from the $^4S_{3/2}$ level and CR involving ions in the $^4I_{9/2}$ and $^4S_{3/2}$ states.[15,16] Therefore, in the experiments at 980 nm, the contribution for the PL signals is mainly due to isolated ions as well

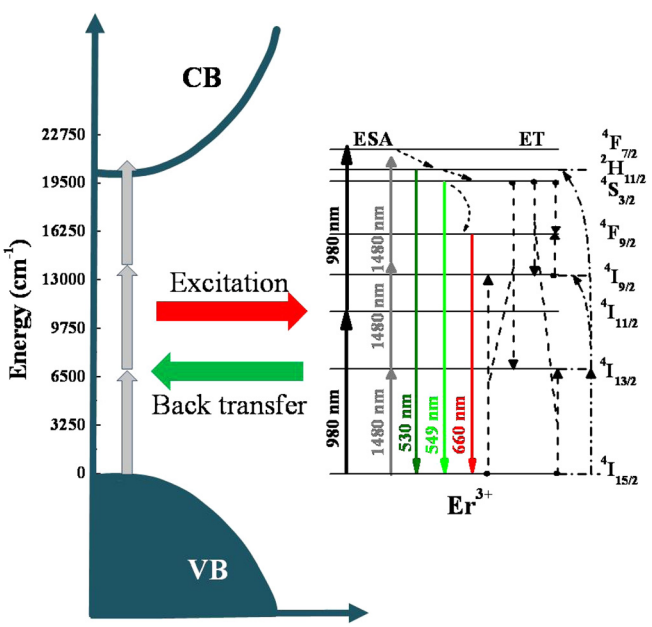

FIG. 4. Simplified energy levels of Er^{3+} ions. The bold upward arrows represent the laser induced transitions. The downward arrows represent luminescence and the dotted arrows represent energy transfer between ions. Also presented is a scheme of conduction and valence bands of the host matrix.

as a fraction of the total number of ions that interact weekly with their neighbors.

For excitation at 1480 nm, the absorption transition $^4I_{15/2} \rightarrow {}^4I_{13/2}$ takes place but the promotion from the $^4I_{13/2}$ level to the high energy states is negligible because the laser wavelength is not resonant with transition $^4I_{13/2} \rightarrow {}^4I_{9/2}$. However, it is probable that two Er^{3+} ions in the state $^4I_{13/2}$ transfer their energy to a third ion, already in the state $^4I_{13/2}$, that is promoted to the state $^2H_{11/2}$; the corresponding excitation pathway is indicated in Fig. 4 by the dashed-dotted lines. This is the most probable pathway for samples having Er^{3+} concentration of 0.1 mol. % and larger, as demonstrated for other glasses.[13,14,17,18] PL at 530 nm ($^2H_{11/2} \rightarrow {}^4I_{15/2}$) is observed as well as at 549 nm ($^4S_{3/2} \rightarrow {}^4I_{15/2}$) that occurs after NR decay from $^2H_{11/2}$ to the $^4S_{3/2}$ state. Since the contribution of isolated ions is negligible the whole PL spectrum is weaker than the spectrum observed for excitation at 980 nm.

In order to understand the discrepancy between the intensity ratio $R = I_{549\ nm}/I_{530\ nm}$ for excitation at 980 nm and 1480 nm, we recall that R depends on the ratio between the amplitudes of transitions $^2H_{11/2} \rightarrow {}^4I_{15/2}$ and $^4S_{3/2} \rightarrow {}^4I_{15/2}$ as well as on the number of Er^{3+} ions in the states $^2H_{11/2}$ and $^4S_{3/2}$. Since only the interacting ions contribute for the UC signal when the sample is excited at 1480 nm, the oscillator strengths of the transitions should be affected in different ways with respect to the case of the isolated ions that participates in the UC for excitation at 980 nm.

B. Pulsed laser excitation at 980 nm and 1480 nm

The UC process excited with a pulsed laser at 980 nm in the GGS-GLASS was previously reported in Ref. 9 and the results obtained in the present experiment were similar. The signal corresponding to transition $^2H_{11/2} \rightarrow {}^4I_{15/2}$ presents a rise time of ≈188 ns attributed to the NR decay from the level $^4F_{7/2}$; the decay time of the signal from states $^2H_{11/2}$ and $^4S_{3/2}$ was ≈24 μs and ≈31 μs, respectively. These values are smaller than the radiative lifetime, calculated using the Judd-Ofelt theory[9] and indicate relevant contributions of NR processes such as ET among the Er^{3+} ions, CR and multiphonon relaxation. We recall that, in general, the measured lifetime of RE levels for Stokes and anti-Stokes excitation are not equal due to the nonequivalent ions inside the inhomogeneous bandwidth and/or the Stark sublevels that participate in the processes. For example for the GGS-GLASS, the $^4S_{3/2}$ level lifetime for the excitation at 532 nm was 25 μs.[9]

In order to identify the UC pathway for pulsed excitation at 1480 nm, the PL spectra were studied with respect to the laser intensity dependence and time behavior. The dependence of the PL intensity versus the laser intensity was cubic indicating that three laser photons are absorbed for each emitted UC photon. The ET process involving three excited Er^{3+} ions, described in Sec. III A, is not probable because the excitation occurs during each laser pulse while in the experiment with CW lasers there is dominance of the ET between the ions due to the large lifetime of levels $^4I_{13/2}$ and $^4I_{9/2}$.

Two possible ways to reach the $^2H_{11/2}$ level may be considered. One possibility is the direct excitation of the Er^{3+} ions: the resonant one-photon absorption $^4I_{15/2} \rightarrow {}^4I_{13/2}$, followed by the two-photon absorption transition $^4I_{13/2} \rightarrow {}^2H_{11/2}$ without real intermediate resonant level. Other possible way is the three-photon absorption (3PA) by the host matrix followed by ET to the Er^{3+} ions. With basis on the temporal behavior of the UC signals described below, we could identify that the 3PA is the more efficient process.

Fig. 5 shows the PL spectra of the GGS-GLASS and the GGS-GC for pulsed excitation at 1480 nm. Notice a splitting of the PL bands in the GGS-GC indicating that the Er^{3+} ions participating in the UC process are located in the crystalline phase. The weak PL signal observed for the GGS-GC is understood considering: (1) the small fraction of the total number of Er^{3+} ions inside the nanocrystals; (2) the time behavior of the PL signals shown in Fig. 6 that indicates larger NR relaxation of the Er^{3+} ions in the GGS-GC. As discussed below the smaller band gap of the GGS-GC favors a larger energy back transfer (EBT) rate from the Er^{3+} ions to the host. These considerations support the statement that the Er^{3+} ions contributing for UC in the pulsed experiment are not the same ions probed in the CW experiment and explain why the splitting of the PL bands are not observed in Fig. 2.

The time evolution of the UC signals, recorded using a detection system having response of ≈10 ns, is illustrated in Fig. 6. Figs. 6(a) and 6(b) show the PL signals associated to transitions $^4S_{3/2} \rightarrow {}^4I_{15/2}$ and $^4F_{9/2} \rightarrow {}^4I_{15/2}$ for the GGS-GLASS, and Figs. 6(c) and 6(d) refer to the GGS-GC. Notice that the signals grow after the laser pulse and reach a maximum value followed by a decay of several microseconds. The signals corresponding to the GGS-GLASS show two decay time components: fast decay (≤20 μs) and slow decay (>100 μs). However, the slow decay is not observed in the GGS-GC PL signal.

Figs. 6(a) and 6(b) show fits of the expression [exp(−t/τ_r)–Aexp(−t/τ_{d1})–Bexp(−t/τ_{d2})], where τ_r and τ_{d1}, τ_{d2} are the rise and decay times, respectively. The fitting of the $^4S_{3/2} \rightarrow {}^4I_{15/2}$ signal provided $\tau_r = 800$ ns, $\tau_{d1} = 15\mu$s, and $\tau_{d2} = 65$ μs. For the $^4F_{9/2} \rightarrow {}^4I_{15/2}$ transition, we determined $\tau_r = 800$ ns, $\tau_{d1} = 20$ μs, and $\tau_{d2} = 950$ μs. The data shown in Figs. 6(c) and 6(d) were fit using [Cexp(−t/τ_r) – Dexp(−t/τ_d)] with

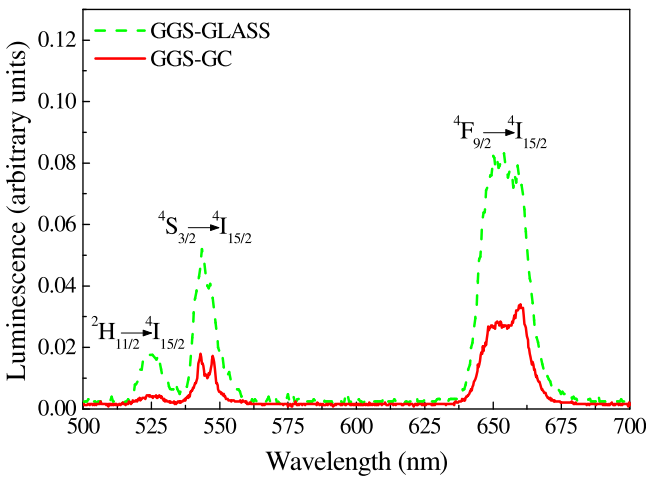

FIG. 5. UC emission spectra under pulsed laser excitation at 1480 nm: GGS-GLASS (green solid line) and GGS-GC (red dashed line).

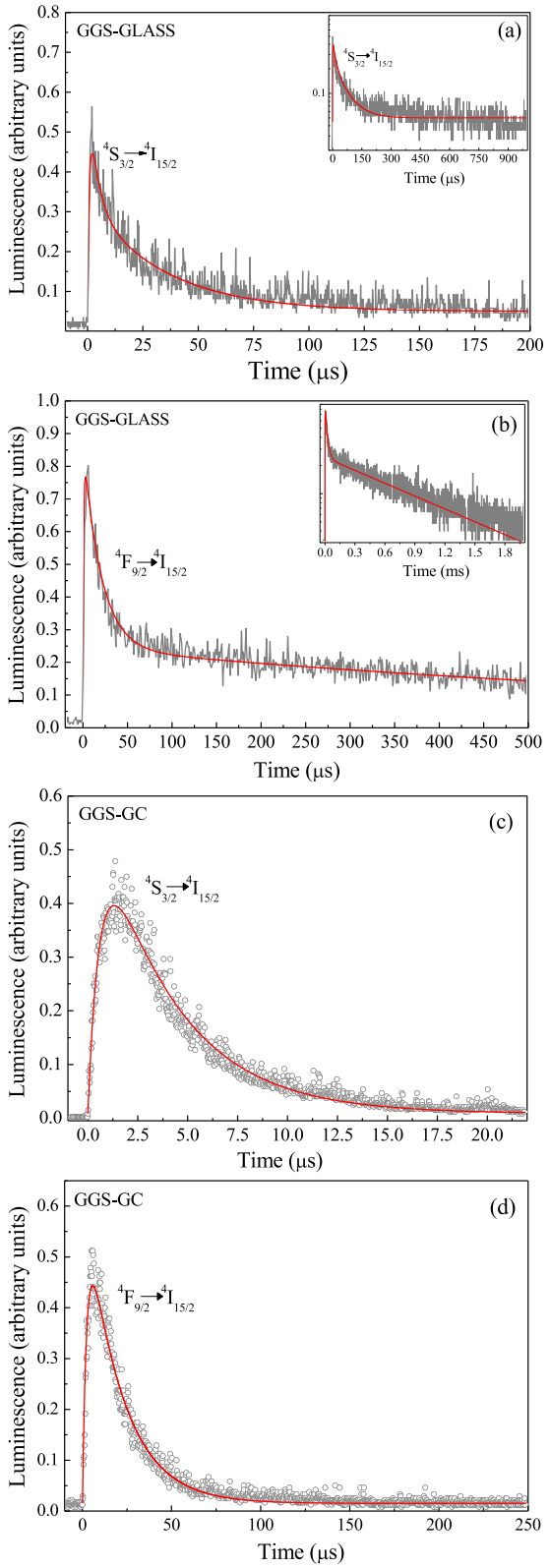

FIG. 6. Dynamics of the UC signal for excitation at 1480 nm. (a) and (b): GGS-GLASS; (c) and (d): GGS-GC.

$\tau_r = 600$ ns and $\tau_d = 3.8\ \mu$s for the transition $^4S_{3/2} \rightarrow {}^4I_{15/2}$ and $\tau_r = 2\ \mu$s and $\tau_d = 20\ \mu$s for the transition $^4F_{9/2} \rightarrow {}^4I_{15/2}$.

The temporal behavior indicates that the direct excitation of the Er^{3+} ions can be ruled out because this process would correspond to ≈5 ns signal rise time. Therefore we concluded that the 3PA by the host matrix followed by ET to the Er^{3+} ions is the dominant pathway and it is relevant because of the large excitation intensity obtained with the pulsed laser (1.34 GW/cm^2).

To model the PL decay from level $^4S_{3/2}$ we recall that τ_d is determined by radiative (W_R) and nonradiative (W_{NR}) probability rates in such way that $\tau_d{}^{-1} = W_R + W_{NR}$. The values of W_R are obtained from Ref. 9. Generally, W_{NR} includes contributions from multi-phonon relaxation and CR with probability rates W_{MP} and W_{CR}, respectively. In a multi-phonon relaxation process, the energy stored in the RE ion is released to the host by emission of p phonons of energy $\hbar\omega$. On the other hand, the efficient CR processes ($^4S_{3/2}$; $^4I_{15/2}$) → ($^4I_{13/2}$; $^4I_{9/2}$) and ($^4S_{3/2}$; $^4I_{15/2}$) → ($^4I_{9/2}$; $^4I_{13/2}$) were reported for Er^{3+} doped glasses and crystals by various authors.[15–18] In the present case, due to the proximity between the $^4S_{3/2}$ level energy and the host band edge an extra term related to the energy back transfer probability, W_{EBT}, from the excited Er^{3+} ions to the host has to be included in such way that $\tau_d{}^{-1} = W_R + W_{MP} + W_{CR} + W_{EBT}$.

The multi-phonon decay rate[22] can be written as $W_{MP}(T) = B[1 + n(T)]^p e^{-\alpha \Delta E}$, where α and B are phenomenological parameters, $n(T) = [e^{\hbar\omega/kT} - 1]^{-1}$ represents the density number of thermally generated phonons per mode at the absolute temperature T, and k is Boltzmann′s constant. If the energy gap to the next lower energy level is ΔE, the number of phonons emitted will be $p = \Delta E/\hbar\omega$. Notice that although phonons of any energy may be involved in the relaxation process, phonons of larger energy dominate and we considered for the calculations of $W_{MP}(T)$ the maximum phonon energy of our samples (345 cm^{-1}) and the values $B \approx 10^6$ s^{-1} and $\alpha = 2.9 \times 10^{-3}$ cm found in Ref. 23.

Table I presents the values for $\tau_d{}^{-1}$, W_{MP}, and ($W_{CR} + W_{EBT}$) for the GGS-GLASS and the GGS-GC. From the results, we notice that the value of $W_{CR} + W_{EBT}$ is larger for the GGS-GC sample. The increase with respect to the GGS-GLASS is attributed to the smaller band gap of the glass-ceramic sample and because the Er^{3+} ions participating in the UC process are located inside the nanocrystals. We recall that $W_{EBT} = 3 \times 10^5$ s^{-1} was determined in Refs. 19–21 by analyzing the light induced conductivity of samples containing 1.8 at. % of Er^{3+} ions. The values obtained here have an approximate order of magnitude. Notice also that the value of W_{NR} corresponding to state $^4F_{9/2}$ does not change due to the heat-treatment of the GGS-GLASS because the energy of this state is smaller than E_g.

TABLE I. Decay time (τ_d) and (W_{MP}—multi-phonon; W_{CR}—cross-relaxation; W_{EBT}—energy back transfer) relaxation rates corresponding to transitions $^4S_{3/2} \rightarrow {}^4I_{15/2}$ and $^4F_{9/2} \rightarrow {}^4I_{15/2}$. The values of $\tau_d{}^{-1}$ for the GGS-GLASS refer only to the fast decay part.

Sample	$\tau_d{}^{-1}$ (10^3 s^{-1})	W_{MP} (s^{-1})	$W_{CR} + W_{EBT}$ (10^3 s^{-1})
GGS-GLASS			
$^4S_{3/2} \rightarrow {}^4I_{15/2}$	66.7 ± 3.3	114 ± 6	60.3 ± 3.0
$^4F_{9/2} \rightarrow {}^4I_{15/2}$	50.0 ± 2.5	349 ± 18	43.2 ± 2.2
GGS-GC			
$^4S_{3/2} \rightarrow {}^4I_{15/2}$	263.2 ± 13.2	114 ± 6	256.8 ± 12.8
$^4F_{9/2} \rightarrow {}^4I_{15/2}$	50.0 ± 2.5	349 ± 18	43.2 ± 2.2

IV. SUMMARY

In summary, we investigated the luminescence behavior of Er^{3+}-doped $Ga_{10}Ge_{25}S_{65}$ glass and glass-ceramic samples with respect to the laser excitation intensity and the time evolution of the frequency upconverted emissions. CW and pulsed lasers operating at 980 nm and 1480 nm were used. The experiments allowed identification of the mechanisms contributing to the infrared-to-visible wavelength conversion. Frequency upconversion processes involving excited-state-absorption by the Er^{3+} ions, three-photon absorption by the matrix host followed by ET to the Er^{3+} ions, and energy transfer among Er^{3+} ions, were characterized. Besides the relaxation mechanisms of energy transfer among the erbium ions and multi-phonon decay, our results indicate an important contribution of energy back transfer from the excited ions to the host that also contributes to reduce of the decay time of the upconverted luminescence.

ACKNOWLEDGMENTS

We acknowledge financial support from the Conselho Nacional de Desenvolvimento Científico e Tecnológico (CNPq) and the Fundação de Amparo à Ciência e Tecnologia do Estado de Pernambuco (FACEPE). The work was performed in the framework of the Photonics National Institute project (INCT de Fotônica) and PRONEX.

[1]F. Auzel, Chem. Rev. **104**, 139 (2004).
[2]M. Yamane and Y. Asahara, *Glasses for Photonics* (Cambridge University Press, Cambridge, 2000).
[3]R. A. H. El-Mallawany, *Tellurite Glasses Handbook—Physical Properties and Data* (CRC, Boca Raton, FL, 2001).
[4]B. J. Eggleton, B. Lutter-Davies, and K. Richardson, Nature Photon. **5**, 141 (2011) and references therein.
[5]N. Mehta, J. Sci. Ind. Res. **65**, 777 (2006).
[6]S. Kasap, K. Koughia, G. Soundararajan, and M. G. Brik, IEEE J. Sel. Top. Quantum Electron. **14**, 1353 (2008).
[7]V. K. Rai, C. B. de Araújo, Y. Ledemi, B. Bureau, M. Poulain, and Y. Messaddeq, J. Appl. Phys. **106**, 103512 (2009).
[8]V. K. Rai, C. B. de Araújo, Y. Ledemi, B. Bureau, M. Poulain, X. H. Zhang, and Y. Messaddeq, J. Appl. Phys. **103**, 103526 (2008).
[9]M. L. Frej, E. Valdez, C. B. de Araújo, Y. Ledemi, and Y. Messaddeq, J. Appl. Phys. **108**, 093514 (2010).
[10]R. Balda, S. Garcia-Revilla, J. Fernández, V. Seznec, V. Nazabal, X. H. Zhang, J. L. Adam, M. Allix, and G. Matzen, Opt. Mater. **31**, 760 (2009).
[11]C. G. Lin, L. Calvez, M. Rozé, H. Tao, X. H. Zhang, and X. J. Zhao, Appl. Phys. A **97**, 713 (2009).
[12]Y. Ledemi, B. Bureau, L. Calvez, M. Le Floch, M. Rozé, C. Lin, X. H. Zhang, M. Allix, G. Matzen, and Y. Messaddeq, J. Phys. Chem. B **113**, 14574 (2009).
[13]C. B. de Araújo, L. S. Menezes, G. S. Maciel, L. H. Acioli, A. S. L. Gomes, Y. Messaddeq, A. Florez, and M. A. Aegerter, Appl. Phys. Lett. **68**, 602 (1996).
[14]D. M. da Silva, L. R. P. Kassab, S. R. Luthi, C. B. de Araújo, A. S. L. Gomes, and M. J. V. Bell, Appl. Phys. Lett. **90**, 081913 (2007).
[15]V. Q. Shi, M. Bass, and M. Birnbaum, J. Opt. Soc. Am. B **7**, 1456 (1990).
[16]A. Lupei, V. Lupei, S. Georgescu, I. Ursu, V. I. Zhekov, T. M. Murina, and A. M. Prokhorov, Phys. Rev. B **41**, 10923 (1990).
[17]R. El-Mallawany, A. Patra, C. S. Friend, R. Kapoor, and P. N. Prasad, Opt. Mater. **26**, 267 (2004).
[18]H. T. Amorim, M. T. de Araujo, E. A. Gouveia, A. S. Gouveia-Neto, J. A. Medeiros Neto, and A. S. B. Sombra, J. Lumin. **78**, 271 (1998).
[19]T. Yu. Ivanova, A. A. Man′shina, A. V. Kurochkin, Yu. S. Tver'yanovich, and V. B. Smirnov, J. Non-Cryst. Solids **298**, 7 (2002).
[20]A. Tverjanovich, Ya. G. Grigoriev, S. V. Degtyarev, A. V. Kurochkin, A. A. Man′shina, T. Yu. Ivanova, A. Povolotskiy, and Yu. S. Tveryanovich, J. Non-Cryst. Solids **326&327**, 311 (2003).
[21]T. Yu. Ivanova, A. A. Man′shina, A. V. Povolotskiy, Yu. S. Tver'yanovich, S.-K. Liaw, and Y.-S. Hsieh, J. Phys. D: Appl. Phys. **41**, 175110 (2008).
[22]R. S. Quimby and B. G. Aitken, J. Non-Cryst. Solids **320**, 100 (2003).
[23]J. Heo and Y. B. Shin, J. Non-Cryst. Solids **196**, 162 (1996).